Analysis of wave- diffusion transitions in the Young's topological interferometer

By

Elizabeth Saldivia Gómez

Thesis submitted in partial fulfillment of the requirements
for the degree of

Doctor of Optics

at the

Instituto Nacional de Astrofísica Óptica y Electrónica
February 2024
Tonanzintla, Puebla

Advisored:
Dr. Gabriel Martínez Niconoff
INAOE

To Co-Cosas

Acknowledgements

Agradezco enormemente a mi madre, porque sus enseñanzas fueron mi motivacion e impetú.
Gracias a la familia que tuve la oportunidad de elegir a lo largo del camino, su apoyo siempre ha sido constante e incondicional.
Finalmente gracias a mi asesor por compartir sus ideas, su conocimiento, su amistad y su paciencia durante estos años de maestria y doctorado, y gracias al CONACYT por el apoyo brindado para la realizacion de este trabajo, y de varios mas.

Contents

Abstract

In this work, the physical properties that occur in the vicinity of the focal regions are analyzed, particularly in places where the irradiance function acquires properties similar to mechanical particles. As a prototype, interferometric systems in which the boundary condition is controlled are described, and multivalued phase regions are identified. This enables us to establish a connection between the phase function and a vector field, providing insight into the physical phenomena linked to the irradiance distribution.

Resumen

En este trabajo se analizan las propiedades físicas que ocurren en la vecindad de las regiones focales, de manera particular en los lugares donde la función de irradiancia adquiere propiedades similares a partículas mecánicas. Como prototipo, se describen sistemas interferométricos en los cuales, controlando la condición de frontera, se identifican regiones multivaluadas de fase. Esto nos permite asociar un campo vectorial a la función de fase y describir el comportamiento físico asociado a la distribución de irradiancia.

Objective

To analyze and describe the wave-diffusion transition processes that occur during the propagation of an optical field and under what conditions such effects can be induced. The study is carried out through the calculation of the dispersion function. This allows for a physical analysis of focal regions as areas of organization of wave phenomena. In particular, self-regulated processes are examined involving the study of the physics of interfered fields.

Chapter 1

Introduction

It begins with the relativity principle, which says that the laws of nature must remain invariant, independently of any frame of reference; this was very important to the posterior development of mathematical optics because the variational principle, used to explain the geometrical approach, automatically satisfies this condition [1]. Originally, the variational principle has a mechanical origin; the link between the mechanical problem and the light description was the Jacobi principle.

Interesting physical properties may appear during the spatial/temporal evolution of the optical field. A very well-known phenomenon that appears during light propagation is the diffraction effect. The diffraction consists of a redistribution of the amplitude and phase of the optical field; when the field is compressed, the phase changes; one example of this is known as the Gouy phase; if the phase function collapses, we say that the adiabatic phase appears [2].

A relevant part of this work is the study of the wave-diffusion optical transitions, and the conditions under this are possible, through an extremal analysis we will prove that in the neighborhood of the focusing regions it is possible to identify like-electrical charge behavior; from this, we can say that the focusing region acts as a source or as a sink for the optical structure fields.

The focusing region is defined as the optical region formed by the envelope of a trajectory family; over this kind of region, important physical effects emerge, for example, wave-diffusion phenomena. The analysis can be implemented using the Green method function; from this, the dispersion relation function will be derived, and it is possible to deduce that the diffusive effect is the primary behavior in the focusing region; this implies complex values of the phase function and an evanescent behavior. During this transition, self-regulated phenomena are present and are modeled by a logistic model with harvesting terms.

This work analyzes the physics that takes place in the neighborhood of the

focusing regions and puts particular attention to the places where the irradiance function acquires like-mechanical particle properties, in interferometric systems; where changing the curvature of the boundary condition function was possible to identify 3 kinds of region in the interference pattern; which, until our background information, this was not reported before.

Also, we examine the case where the focusing region is generated in a random index refraction media, obtaining like-solitonic/vortex behavior, which is consistent with the diffusive transition because it implies the "stretching" of the caustic.

In Chapter 2 we describe the theoretical background of the work, review the mathematical tools that we will use, and give an introduction to the problem under consideration; in Chapter 3 we do a brief review of the calculus of the Green solution to the diffraction problem, we obtain the dispersion relation function in the limit of the wave- diffusion transition, in Chapter 4, the results of the focusing regions in a dynamical media will be presented, in chapter 5 the generalized Young interferometer is addressed using the Airy and Pearcy functions as a prototype, demonstrate, first, that the caustic region acts as attractor/sink for the interference fringes, second, the focusing region generates irradiance flow redistribution through interference fringes until all the pattern gets uniform energy. Finally, in Chapter 6 the conclusions are enounced and future work is presented. For the study of the global interference pattern, we associate the phase function with a vector field, driven by the curvature function, this proposal being analogous to the Ricci flow.

Chapter 2

Mathematical generalities in the light propagation

2.1 Geometrical approach

One of the most valuable concepts in optics involves visualizing light as a collection of geometric paths. This approach has proven essential to solving practical problems and to improving our understanding of various phenomena. However, it is important to recognize that light is fundamentally an electromagnetic phenomenon. The geometric perspective becomes particularly useful when the wavelength of light is significantly smaller than the scales at which the material properties, such as frequency ν and refractive index n, exhibit noticeable variations. In other words, this perspective is valid when we are operating within the scale where medium inhomogeneities become apparent. Within this context, optical laws can be formulated in a purely geometric manner. However, it is crucial to keep in mind that this is an approximation, and it becomes less accurate when the mentioned conditions are not satisfied, as wave effects then become impossible to disregard.

In geometric optics, the energy is considered transported along certain curves (light rays), and these curves or light rays have the property of always being perpendicular to the wavefronts, defined as constant phase surfaces Fig.2.2.

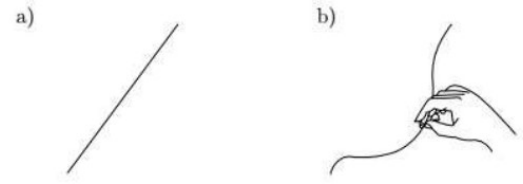

Figure 2.1: The effect of a refractive index that not have a constant value.

Around 1621 Snell found experimentally that the sine of the 'angle of incidence' and the 'angle of refraction' have a relationship that depends only on the two media involved, in 1661 Fermat shows that when light propagates through a medium, its speed changes according to the optical density of the medium or refractive index; In free space (the speed of light has a constant value) or in any medium whose refractive index has a constant value, light rays propagate in a straight line, when the medium is different, light travels m slowly, and the rays follow curved paths that according to Fermat are paths whose optical path length has a minimum value [3] and with this he deduces Snell's law.

However, some drawbacks with this principle were soon noticed, since the law of reflection was sometimes consistent with the path in which the propagation time was greatest, therefore the rays. that obey the law of reflection occasionally minimize or maximize their travel time, apparently economizing time [4], these difficulties were eliminated by expanding the "principle of minimum time" al "stationary time principle" or "Fermat principle", in which the aforementioned cases and those in which the propagation time turned out to have a stationary value are already considered. The mathematical construction of the "stationary time principle" is due to Joseph L. Lagrange and Leonhard Euler [5], who developed variational calculus as a method to find curves that minimize or maximize some integrals.

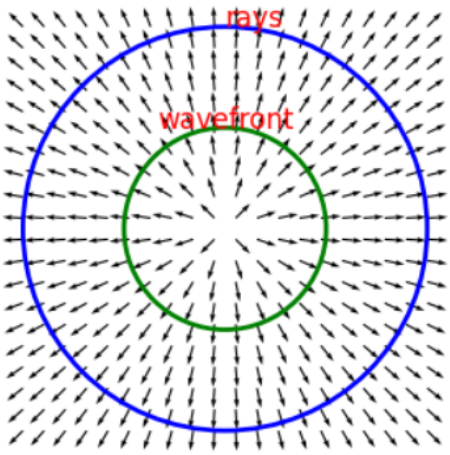

Figure 2.2: The trajectories (rays) are perpendicular to the wavefront.

The construction of this last family of trajectories is parallel to the construction of orthogonal trajectories of the surface a $S = const$ as follows: the surface of equal time in optics is analogous to the surface of equal action in mechanics; the Fermat principle of least time is the optical interpretation of the principle of least action or Jacobi principle [1].

From this point is possible to say that the rays of light describe different types

of curves in the 3D space, but this is so hard if we try to express it from the classic fixed reference system; historically, to make this description easier, the curve is described from a reference system that is moving over a curve in the three-dimensional space, the mathematical expression of this is a set of differential equations known as the Frenet-Serret equations.

2.2 Serret- Frenet equations

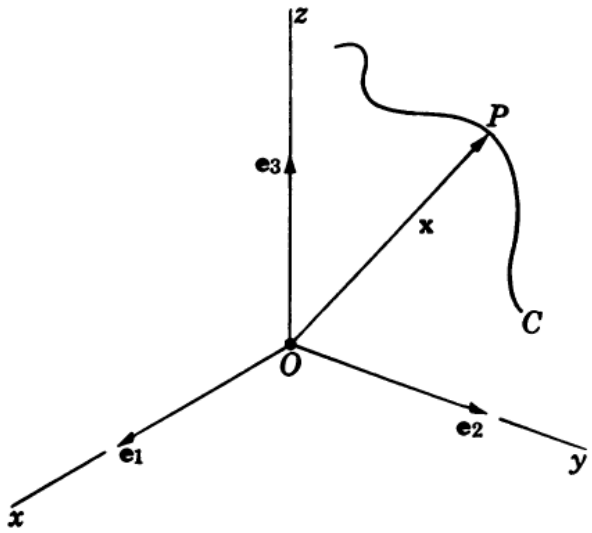

Figure 2.3: A curve in the 3D space.

Suppose that e_i, e_j, e_k are the unitary vectors in the positive direction of the x, y, and z axes, from the Fig.2.3, is possible to describe the curve $\mathbf{C}$ as the the radius vector $\vec{AB} = \mathbf{x}$ of a point P as a function of u in the following way:

$$\mathbf{x} = x_i e_i + x_j e_j + x_k e_k \tag{2.1}$$

Where P is not only $P(x_i)$, is also $P(\mathbf{x})$ or $P(u)$. Thus the length of the vector $\mathbf{x}$ is given by

$$|\mathbf{x}| = \sqrt{x_1^2 + x_2^2 + x_3^2}. \tag{2.2}$$

the arc length of a segment of the curve between points $A\,(u_0)$ and $P(u)$ can be calculated by means of:

$$s(u) = \int_{u_0}^{u} \sqrt{\dot{x}^2 + \dot{y}^2 + \dot{z}^2}du = \int_{u_0}^{u} \sqrt{\dot{\mathbf{x}} \cdot \dot{\mathbf{x}}}du. \tag{2.3}$$

. The dot in Eq.(2.4) indicates differentiation with respect to u, which implies

that the arc length s is always positive. This means that the curve is oriented and increases with increasing u..

The arc length remains the same when the parameter on the curve is altered from u to u_1, and this invariance can be expressed by substituting Eq. (2.4) with the equation.

$$ds^2 = dx^2 + dy^2 + dz^2 = d\mathbf{x} \cdot d\mathbf{x}, \tag{2.4}$$

which is independent of u. We can substitute s for u as a parameter, which is valid since $ds/du \neq 0$. This is demonstrated in Eq. (2.5).

$$\frac{d\mathbf{x}}{ds} \cdot \frac{d\mathbf{x}}{ds} = 1 \tag{2.5}$$

we can see that the vector $d\mathbf{x}/ds$ is a unit vector, the geometrical interpretation is as follows: The vector $\Delta\mathbf{x}$ joins two points $P(\mathbf{x})$ and $Q(\mathbf{x} + \Delta\mathbf{x})$ on the curve. The vector $\Delta\mathrm{x}/\Delta s$ has the same direction as Δx and for $\Delta s \to 0$ passes into a tangent vector at P

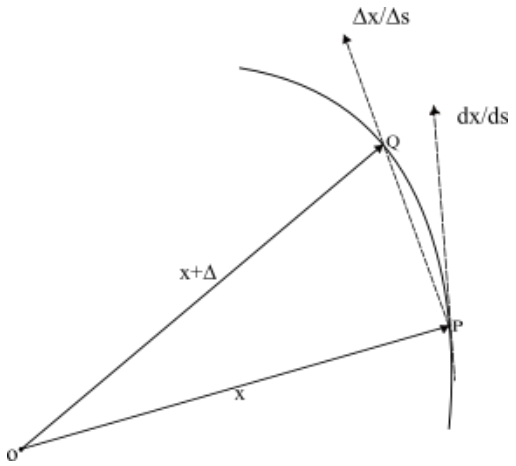

Figure 2.4: Arc lenght between P and Q points .

Due to the lenght is equal to 1, the unit tangent vector to the curve at point P is given by:

$$\mathbf{t} = \frac{d\mathbf{x}}{ds} \tag{2.6}$$

we can say that in the limit, when $P \to Q$, the tangent passes through two consecutive points on the curve [6]. The plane that passes through 3 consecutive points of the curve is called the *osculating plane* and is defined by

$$\mathbf{X} = \mathbf{x} + \lambda\dot{\mathbf{x}} + \mu\ddot{\mathbf{x}}, \quad \lambda, \mu \text{ arbitrary constants} \tag{2.7}$$

The line perpendicular to the tangent line at point P in the osculating plane is called the *principal normal*, in this direction we place a unit vector $mathbfn$, the sense of which may be arbitrarily selected, provided it is continuous along the curve. Taking the arc length as parameter, we have:

$$\mathbf{x} = \mathbf{x}(s), \quad \mathbf{t} = d\mathbf{x}/ds = \mathbf{x}', \quad \mathbf{t} \cdot \mathbf{t} = 1 \tag{2.8}$$

prime means differentiation respect to s, then we obtain by differentiating $t \cdot t = 1$:

$$t \cdot t' = 0 \tag{2.9}$$

This shows that the vector $\mathbf{t}' = d\mathrm{t}/ds$ is perpendicular to t, and since

$$\mathbf{t} = \mathbf{x}' = \dot{\mathbf{x}}u', \quad \mathbf{t}' = \ddot{\mathbf{x}}\left(u'\right)^2 + \dot{\mathbf{x}}u'', \tag{2.10}$$

we see that $\mathbf{t}'$ lies in the plane of $\dot{\mathbf{x}}$ and $\ddot{\mathbf{x}}$, and hence in the osculating plane, introducing a proportionality factor κ

$$\mathbf{k} = d\mathbf{t}/ds = \kappa\mathbf{n}. \tag{2.11}$$

Eq. (2.11) expresses the rate of change of the tangent when we proceed along the curve and is called the *curvature vector* with κ the curvature; $|\kappa|$ is the length of the curvature vector. . The direction of $\mathbf{n}$ can be chosen freely, however the direction of $d\mathbf{t}/ds$ is completely determined by the curve, regardless of its orientation; when s is reversed, t also reverses. If $\mathbf{n}$ is taken in the same direction as $d\mathbf{t}/ds$ (which is often done), then κ is always positive.

Curvature measures the rate of change of the tangent as it moves along the curve. To measure the rate of change of the osculating plane, we use the normal at P to the osculating plane named the binormal. In it we place the unit binormal vector $\mathbf{b}$ since $\mathbf{t}$, $\mathbf{n}$, are mutually perpendicular unit vectors, we define the vector $\mathbf{b}$ as:

$$\mathbf{b} = \mathbf{t} \times \mathbf{n}. \tag{2.12}$$

The vectors $\mathbf{n}$, $\mathbf{t}$, $\mathbf{b}$ form a new reference frame which is moving along the curve and is known as the *moving trihedron*, and satisfies the following:

$$\mathbf{t} \cdot \mathbf{t} = 1, \mathbf{n} \cdot \mathbf{n} = 1, \mathbf{b} \cdot \mathbf{b} = 1, \tag{2.13}$$

$$\mathbf{t} \cdot \mathbf{n} = 0, \mathbf{n} \cdot \mathbf{b} = 0, \mathbf{b} \cdot \mathbf{t} = 0. \tag{2.14}$$

As $\mathbf{t}' = \kappa\mathbf{n}$ and $\mathbf{b}' = -\tau\mathbf{n}$, in order to complete this information, it can be expressed $\mathbf{n}' = d\mathbf{n}/ds$ in terms of the unit vectors of the moving trihedron. Since $\mathbf{n}'$ is perpendicular to $\mathbf{n}$, $\mathbf{n}\cdot\mathbf{n}' = 0$, and we can express $\mathbf{n}'$ linearly in terms of $\mathbf{t}$ and $\mathbf{b}$:

$$\mathbf{n}' = \alpha_1\mathbf{t} + \alpha_2\mathbf{b}. \tag{2.15}$$

Since according to Eq. (2.14) and

$$\alpha_1 = \mathbf{t}\cdot\mathbf{n}' = -\mathbf{n}\cdot\mathbf{t}' = -\mathbf{n}\cdot\kappa\mathbf{n} = -\kappa, \tag{2.16}$$

$$\alpha_2 = \mathbf{b}\cdot\mathbf{n}' = -\mathbf{n}\cdot\mathbf{b}' = +\mathbf{n}\cdot\tau\mathbf{n} = \tau, \tag{2.17}$$

we find for $d\mathbf{n}/ds$:

$$\mathbf{n}' = -\kappa\mathbf{t} + \tau\mathbf{b}. \tag{2.18}$$

The three vector formulas known as the Serret- Frenet formulas:

$$\frac{d\mathrm{t}}{ds} = \kappa\mathbf{n} \tag{2.19}$$

$$\frac{d\mathbf{n}}{ds} = -\kappa\mathrm{t} + \tau\mathbf{b} \tag{2.20}$$

$$\frac{d\mathbf{b}}{ds} = -\tau\mathbf{n} \tag{2.21}$$

The three planes formed by the three sides of the moving trihedron are called: the osculating plane, through the tangent and principal normal, with equation $(y-x)\cdot b = 0$, the normal plane, through principal normal and binormal, with equation $(y-x)\cdot t = 0$ and the rectifying plane, through binormal and tangent, with equation $(y-x)\cdot n = 0$.

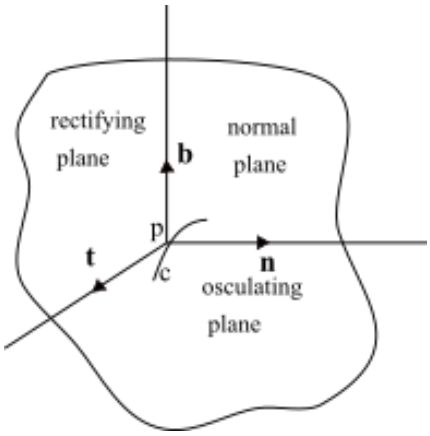

Figure 2.5: Frenet Serret reference system.

2.3 Diffraction

2.3.1 Huygens- Fresnel principle

The physical phenomenon that occurs when the light finds an obstruction during its propagation is known as diffraction and can be aboard by two ways, the first one is the Huygens- Fresnel principle, which says that every point of the wavefront can be described as point source of spherical waves, so, the field that emerges later the obstruction is the superposition of these spherical waves.

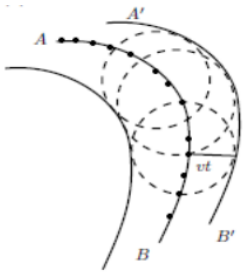

Figure 2.6: Spherical waves emerge from a set of point sources over the wavefront

Mathematically was developed by Kirchoff, Rayleigh and Sommerfeld through the diffraction integral:

$$\phi_1 = \iint U_1(x_1, y_1) \exp(ikr) dx_1 dy_1 \tag{2.22}$$

where $U_1(x_1, y_1)$ is the amplitude and phase of the wave that emerge from (x_1, y_1) and $1/i\lambda z$ is a constant value. The field in the x_2y_2 plane is given by:

$$U_2(x_2, y_2) = \frac{1}{i\lambda z} \iint U_1(x_1, y_1) \exp(ikr) dx_1 dy_1 \tag{2.23}$$

2.3.2 Angular spectrum model

Very close to the Huygens- Fresnel principle, the angular spectrum model proposes that any optical field can be described as a set of plane waves whose propagation vectors are in distinct directions and satisfies the wave equation given by:

$$\nabla^2 \Psi = \frac{1}{c^2} \frac{\partial^2 \Psi}{\partial t^2} \tag{2.24}$$

The classic solution consists of separating the spatial components from the temporal ones, proposing a solution of the form:

$$\Psi(x, y, z, t) = \psi(x, y, z) \exp^{i\omega t} \tag{2.25}$$

substituting ((2.25)) in ((2.24)) we obtain the equation for the complex amplitude of the Helmholtz wave or equation:

$$\nabla^2 \psi(x, y, z) + k^2 \psi(x, y, z) = 0 \tag{2.26}$$

where $\vec{k}$ is the wave direction vector; The simplest solution to this equation is a plane wave represented by:

$$\psi(x, y, z) = Ae^{x\cos\alpha + y\cos\beta + z\cos\gamma} = Ae^{i2\pi(xu+yv+zp)} \tag{2.27}$$

with α, β y γ are the directors angles of $\vec{k}$ such that:

$$u^2 + v^2 + p^2 = \frac{1}{\lambda^2} \tag{2.28}$$

(2.28) represents a sphere in frequency space, for the case in which u, v, p are real. Therefore, the diffraction field, in its modal representation, is expressed as follows.

$$\phi(x, y, z) = \iint A(u, v) e^{i2\pi(xu+yv+zp)} dudv \tag{2.29}$$

where the boundary condition or transmittance function, determined by the diffracting object is given by:

$$\phi(x, y, z = 0) = t(x, y) = \iint A(u, v) e^{i2\pi(xu+yv)} dudv \tag{2.30}$$

t is possible to note that equation ((2.30)) has the form of a Fourier transform, so we can obtain the amplitude distribution by calculating the inverse function:

$$A(u, v) = \iint f(x, y) e^{-i2\pi(xu+yv)} dxdy \tag{2.31}$$

we can obtain the amplitude of the field.

2.4 Introduction to focusing regions

For many years the study of caustics was aboard by catastrophe theory; in large measures, structural stability is a useful mathematical tool for caustics whose topology survives the perturbations, for example, the caustic formed as a result of

refraction or reflection of light by wavy water surface Fig. 2.7 [7].

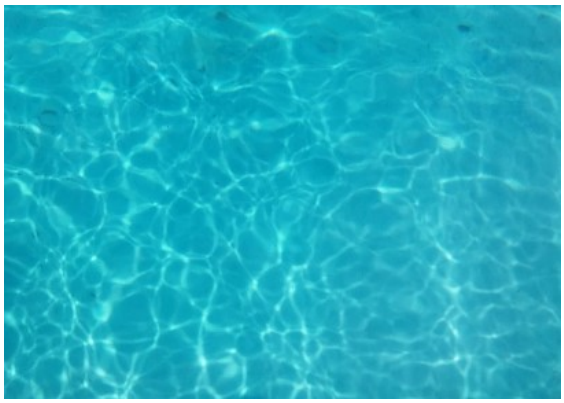

Figure 2.7: weavy

During light propagation, diffraction or focusing are some of the phenomena that may occur; the last effect is characterized by the formation of areas or regions where the light intensity is very high, and non-linear effects can be present. Mathematically, the focusing regions are represented by the envelope of the center of curvature of the boundary condition function Fig. 2.8.

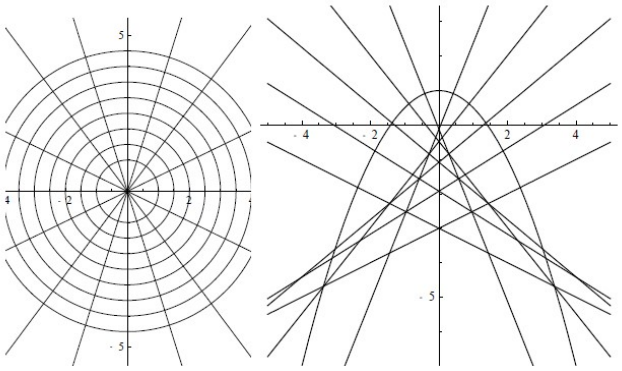

Figure 2.8: envolvente

We are interested in the study of the physical properties of each of the regions in Fig. 3.1 which we will carry out through the study of interference effects.

Two types of interference are proposed:

- Interference with a plane wave.
- Interference with a field of the same species.

Using a Mach-Zehnder interferometer, we obtained the following images that demonstrate different observed effects:

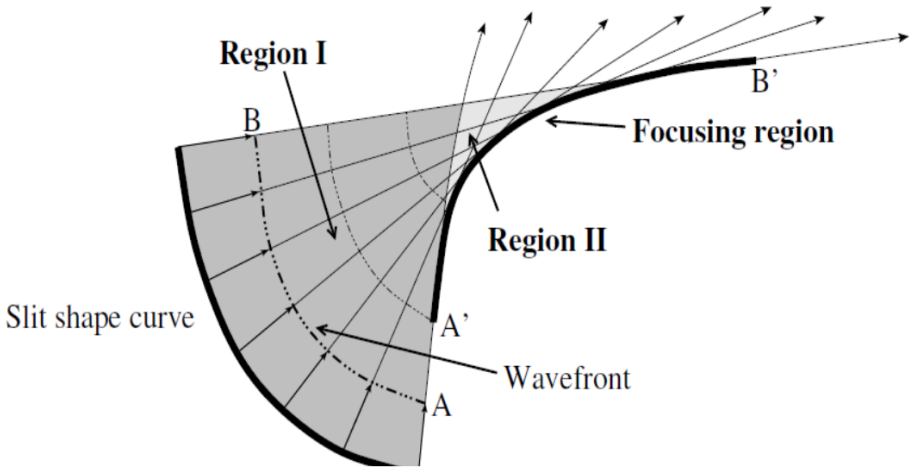

Figure 2.9: Geometric description of a focal region.

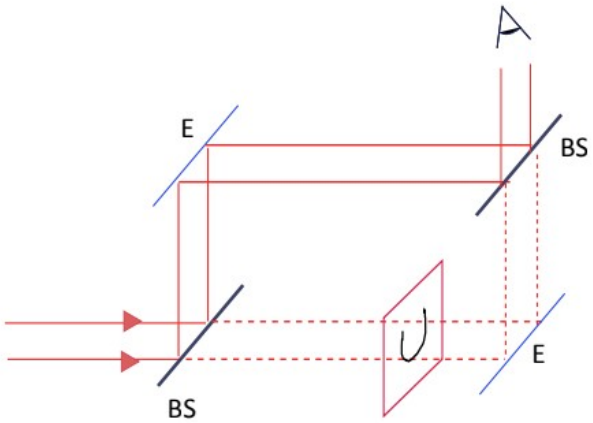

Figure 2.10: Mach zehnder interferometer

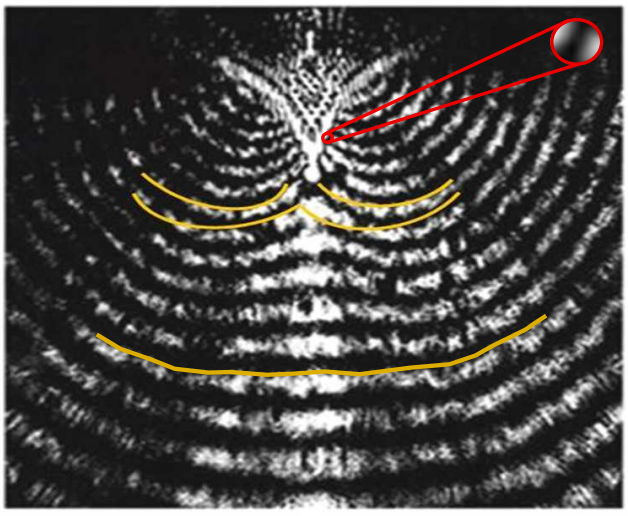

Figure 2.13: Behavior of the optical field in the vicinity of the focal region.

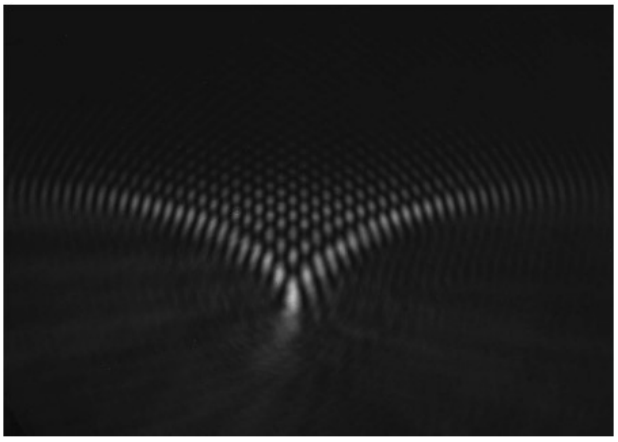

Figure 2.11: [Diffraction from a parabolic slit.

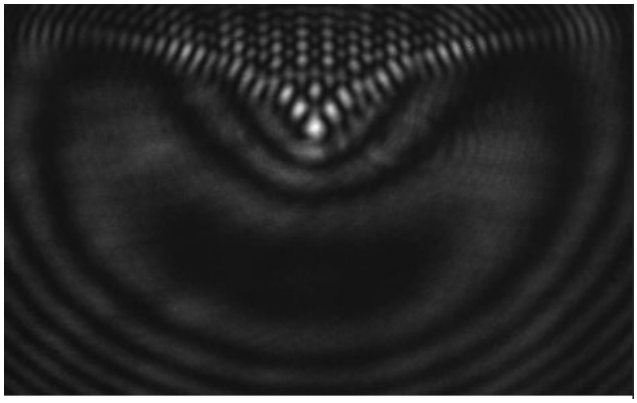

Figure 2.12: Interference from the diffraction of a parabolic slit with a plane wave. Physical effects produced in a Mach Zender interferometer with a parabolic slit in one arm of it.

2.5 Description of the generalized wave equation

From the previous experimental results, important behaviors are identified, one of them is the sink characteristic of the focal regions, and the bifurcation effects, for their study it is convenient to start with the study of the characteristics of the electromagnetic field, beginning with Maxwell's equations:

$$\nabla \times \mathbf{E} = -\frac{\partial \mathbf{B}}{\partial \mathbf{t}} \tag{2.32}$$

$$\nabla \cdot \mathbf{E} = -\frac{\rho}{\epsilon} \tag{2.33}$$

$$\nabla \times \mathbf{B} = \mu \mathbf{J} + \mu\epsilon \frac{\partial \mathbf{E}}{\partial \mathbf{t}} \tag{2.34}$$

$$\nabla \cdot \mathbf{B} = \mathbf{0} \tag{2.35}$$

Through some mathematical manipulations, we arrive at:

$$\nabla^2 E = \mu\sigma\frac{\partial E}{\partial t} + \mu\epsilon\frac{\partial E^2}{\partial t^2} \tag{2.36}$$

The above equation decomposes into 3 scalar equations, one for each component, and they take the form:

$$\nabla^2 \phi_i = b\frac{\partial \phi_i}{\partial t} + \frac{1}{v^2}\frac{\partial {\phi_i}^2}{\partial t^2} \tag{2.37}$$

where $\mu\epsilon = 1/v^2$ y b= $\mu\sigma$.
This is known as the wave-diffusion equation. We are interested in understanding the conditions under which one of the effects becomes predominant.

2.6 Wave- diffusion processes

We are interested under what conditions the diffusive effects are dominant with respect to the wave effects and vice versa, for this, the proposed analysis for a solution of Eq. (2.37) is in the form:

$$\phi = \psi exp(-i\omega t) \tag{2.38}$$

we obtained

$$\nabla^2\psi + (k^2 + ib\omega)\psi = 0 \tag{2.39}$$

in the last v is the wave velocity and b is known as the diffusion parameter. This equation is similar to the Helmholtz equation with complex parameters.

$$k^2 = \xi^2 - \eta^2, \text{where} \quad \sigma = \xi + i\eta \tag{2.40}$$

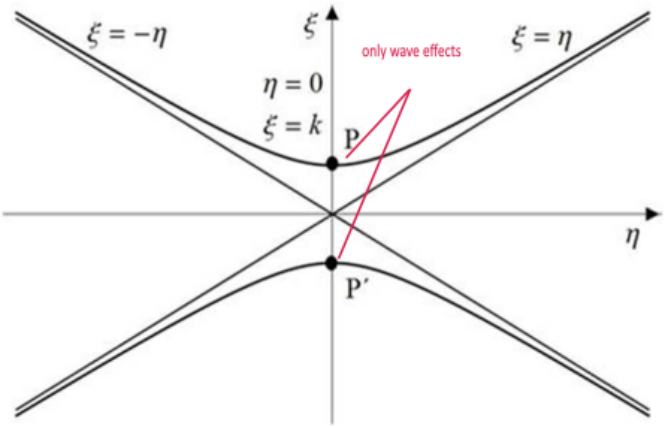

Figure 2.14: Graph of the dispersion relation k.

From the figure is possible identify two limit cases, first, the two points over the ξ axes, which corresponds to the classic case, wave behavior. The other case is where $\xi \to \eta$, which is possible only when the effective refractive index tends to 0, so the resultant equation takes the form:

$$\nabla^2 \phi_d + i\omega b \phi_d = 0 \tag{2.41}$$

Since this solution corresponds to a harmonic solution in time, so we can propose a Green-type solution.

2.7 Green's function method

The Green's function method is widely used to analyze various physical phenomena, including scalar and vector wave fields. This method is based on the premise that, given a geometry, any field satisfying a source distribution, kind Dirac delta function, and arbitrary initial and boundary conditions can be constructed from spatial and temporal integrals. In the case of waves with harmonic time dependence, this method allows us to eliminate the temporal variable from the calculation; this last state allows us to consider only boundary value problems [[8]]. The Green's function, which accounts for both wave and diffusion effects, is given by:

$$\phi(P) = \frac{1}{4\pi} \int\int \frac{e^{i\sigma r}}{r} \left[(-i\sigma - \frac{1}{r})\phi\hat{r} - \nabla\phi \right] \cdot \hat{n} ds, \tag{2.42}$$

recalling that σ is in the form $\sigma = \xi + i\eta = (k^2 + i\omega b)^{1/2}$, substituting it into(2.42), we arrive at:

$$\phi = \frac{1}{4\pi} \int\int \frac{e^{i\sigma r\xi} e^{\sigma r\xi}}{r} \left[(\xi(i-1) - \frac{1}{r})\phi\hat{r} - \nabla\phi \right] \cdot \hat{n} ds, \tag{2.43}$$

where $\eta = \sqrt{\frac{b\omega}{2}}$, equation (**??**) represents the amplitude behavior for the case where the dominant behavior is diffusion. For the diffusive case, as $k \to 0$ the Green's function solution is written as:

$$\begin{aligned} \phi_w(P) = 0 &= lim_{k\to 0} \frac{1}{4\pi} \int\int \frac{e^{ikr}}{r} \left[(ik - \frac{1}{r})\phi\hat{r} - \nabla\phi \right] \cdot \hat{n} ds \\ &= \frac{1}{4\pi} \iint \frac{1}{r} \left(\left(-\frac{1}{r} \right) \phi\hat{r} - \nabla\phi \right) \cdot \hat{n} ds, \end{aligned} \tag{2.44}$$

which implies:

$$\nabla\phi = -\frac{\phi}{r}\hat{r} \tag{2.45}$$

The expression above represents a focal region [9]. Another point of view is the extremal analysis, where we focus our attention on the eikonal equation.

2.8 Focal region: Extreme analysis

The variational principle or the principle of least action determines the geometry of the trajectories that a particle follows, extremizing "the action of all possible trajectories", because the action of a particle s trajectory is mathematically similar to the length of the optical path of a ray of light. light, the principle of least action is the mechanical interpretation of Fermat's principle [5]. Fermat's principle says that the path followed by a ray of causes the optical path length to take an extreme value. Also, we can express the amplitude of the optical field as:

$$\phi = A\exp(iK_0L)\text{con} \quad L = h + ig \tag{2.46}$$

Substituting into the Helmholtz equation and separating the real and imaginary parts,

$$\begin{aligned} \nabla^2 g &= K_0(|\nabla h|^2 - |\nabla g|^2) - \frac{K^2}{K_0} \\ \nabla^2 h &= 2(\nabla h \cdot \nabla g) - \frac{b\omega}{K_0} \end{aligned} \tag{2.47}$$

For the case in which we want to recover only wave effects, this can be achieved by setting $b = 0$ ó $g = 0$, which reduces equations (2.47) to the following expressions:

$$\nabla^2 g = 0 \qquad \text{y} \qquad |\nabla h|^2 = \frac{K^2}{K_0^2} = n^2 \tag{2.48}$$

The above expressions correspond to the well-known models, indicating that the model is consistent with traditional optics.

For the case where diffusive effects are present, we have $K = 0$ and the transversality condition $(\nabla h \cdot \nabla g) = 0$, leading to:

$$\begin{aligned} \nabla h &= | - \frac{b\omega}{K_0} \qquad \text{(a)} \\ \nabla^2 g &= 0 \qquad \text{(b)} \end{aligned} \tag{2.49}$$

The equation 2.49(a) implies that in the region where diffusion processes occur, it behaves like a source for the wave field. A preliminary set of conclusions at this point are:

- Wave-diffusion processes are possible and occur in the vicinity of the focal region of an optical field.
- It was found that wave-diffusion transitions imply a complex wave number.
- Focal regions act as sources or sinks of the field.

Chapter 3

Topological Young interferometer

Given our interest in the study of optical fields and proposing focal regions as areas of organization. A focal region is defined as a region of maximum irradiance (a singularity of the optical field), which can generate non-linear effects. Mathematically, these regions are represented by the envelope of all curvature centers of the boundary condition of the transmittance function. Remember Fig. 3.1, from this is possible to identify 3 kinds of distinct regions as follows:

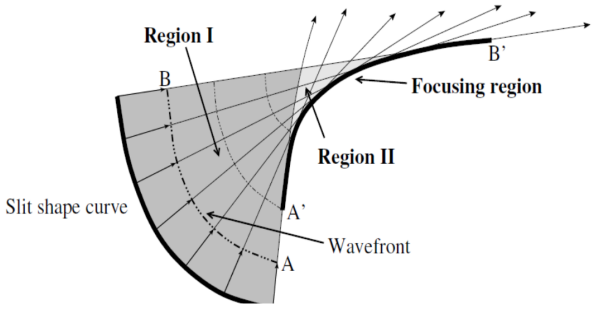

Figure 3.1: Geometric description of a focal region.

- Region I: Univalued phase region.
- Region II: Multivalued phase region, self-induced effects occur.
- Region III: Envelope of all trajectories, field organization zone.

To implement this analysis, we will use the Young interferometer as a prototype.

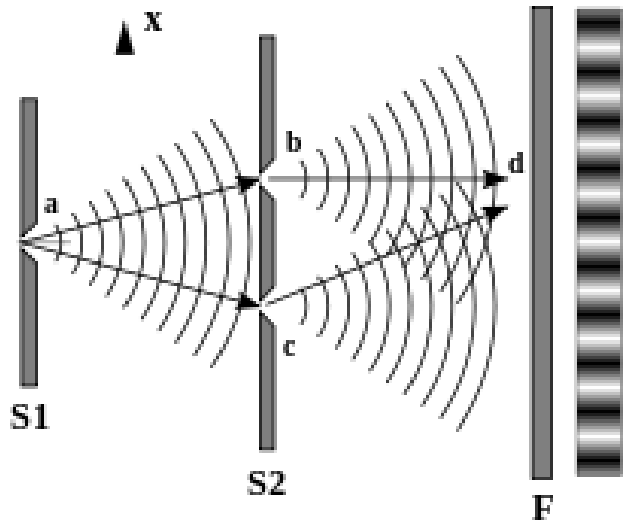

Figure 3.2: Scheme of the Young interferometer.

The main difference between the classical Young interferometer and what we call the topological interferometer is that, in the aperture plane, we apply a "topological" transformation. This transformation generates quadratic and cubic curves, whose diffraction produces an optical field related to Airy beams and Pearcy beams.

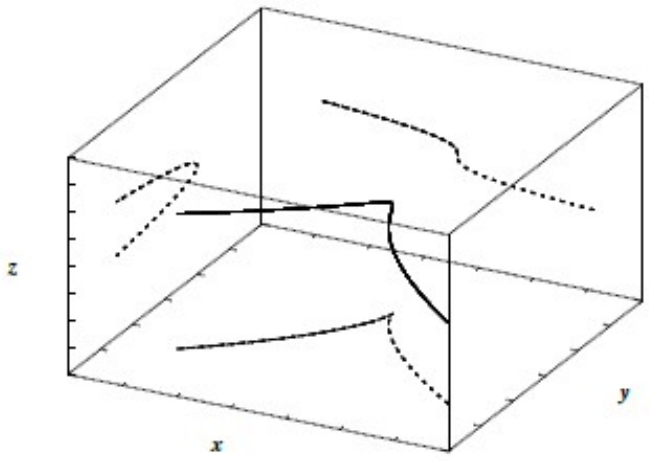

Figure 3.3: Decomposition of a 3D curve in the planes of the trihedral reference system.

We can perform a generic decomposition of the 3D curve using the trihedral reference system, which is mounted on the curve and is independent of the observer.

This decomposition results in a quadratic curve in the osculating plane, a cubic curve in the rectifying plane, and a cusp-like curve in the normal plane. It is important to emphasize that these transformations depend on how the curve is illuminated.

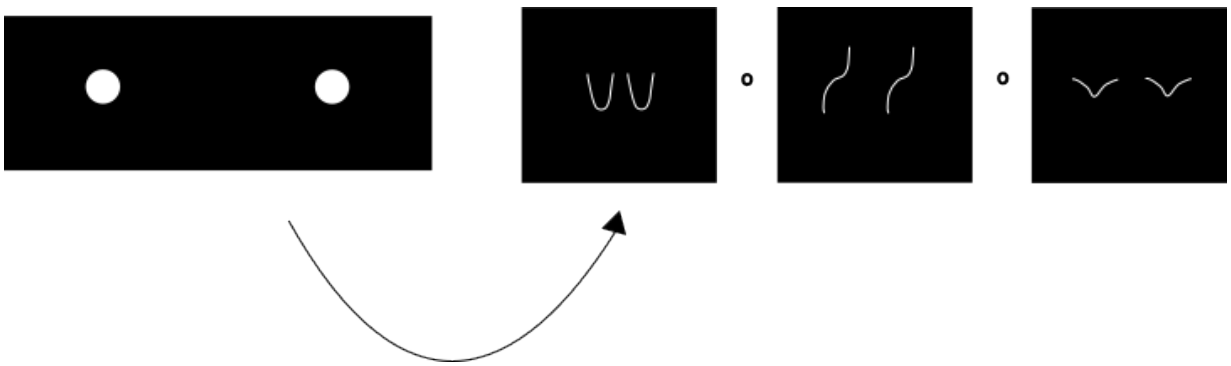

Figure 3.4: Transformations to circular apertures.

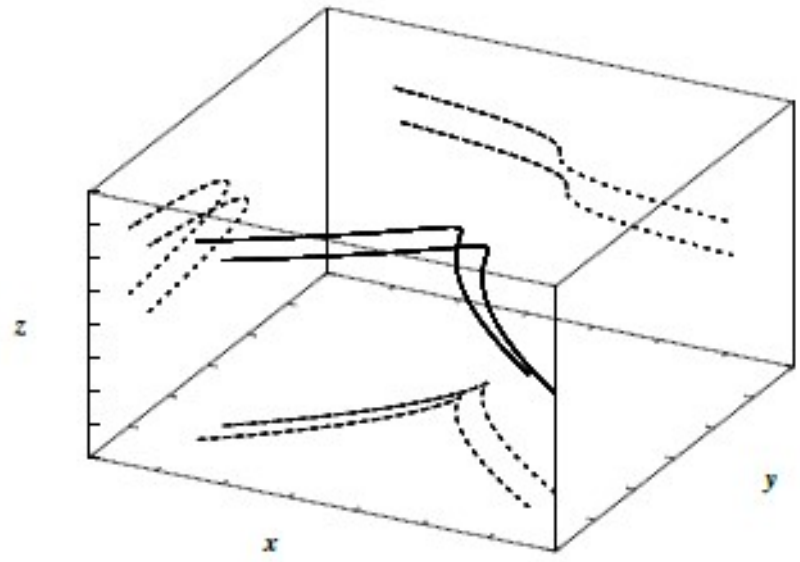

Figure 3.5: Decomposition of the generalized 3D Young interferometer in the osculating, rectifying, and normal planes.

The amplitude of the optical field can be represented as the sum of two spherical

wavefronts; using Euler's identity, the amplitude function can be represented as:

$$\varphi\left(r_1, r_2\right)=\sqrt{A^2+B^2+2AB\cos k\left(|r_1|-|r_2|\right)}\exp\left(i\tan^{-1}\left(i\frac{\operatorname{sink}|r_1|+\operatorname{sink}|r_2|}{\cos k|r_1|+\cos \mathrm{k}|r_2|}\right)\right) \tag{3.1}$$

The expression inside the square root represents the irradiance function, where the argument of the cosine term contains information about the geometry of the interference fringes. It is convenient to rewrite the phase function as:

$$k\left(|\mathbf{r}_1|-|\mathbf{r}_2|\right)=k\left(\frac{\left(\mathbf{r}_1-\mathbf{r}_2\right)\cdot\left(\mathbf{r}_1+\mathbf{r}_2\right)}{|\mathbf{r}_1|+|\mathbf{r}_2|}\right) \tag{3.2}$$

It can be observed that the vector field $\mathbf{r_1}+\mathbf{r_2}$ defines an interference fringe, and the vector field $\mathbf{r_1}-\mathbf{r_2}$ defines the irradiance flow between two neighboring fringes. Interference fringes are accurately described through the envelope of constructive points placed on the ellipses defined by $|\mathbf{r_1}|+|\mathbf{r_2}|=c_j$, where $j=1,2,..n$. Applying a transformation to the transmittance function, we obtain the following.

$$t(x,y)=\delta(y-f(x-a))+\delta(y-f(x+a)), \tag{3.3}$$

Therefore, the amplitude function becomes:

$$\varphi\left(r_{1f}, r_{2g}\right)=\exp\iint_{-\infty}^{\infty}\delta(y-f(x))+\delta(y-g(x))\exp(ikr)dxdy. \tag{3.4}$$

The selected functions are: $f(x)=x^2, x^3, x^{2/3}+y^{2/3}=c$, which generate the Pearcey, Airy, and cusp beams, respectively.

$$\varphi\left(\mathbf{r_{1f}}, \mathbf{r_{2g}}\right)=\int_{-\infty}^{\infty}\sqrt{F(x)}\exp\left(i\tan^{-1}\left(i\frac{\operatorname{sink}|\mathbf{r_1}|+\sin k\left|\mathbf{r_g}\right|}{\operatorname{cosk}|\mathbf{r_1}|+\cos k\left|\mathbf{r_{2g}}\right|}\right)dx\right. \tag{3.5}$$

Considering that now the transmittance function has an associated caustic:

$$k\left(\left|r_{1f}\right|-\left|r_{2g}\right|\right)=k\left(\frac{\left(r_{1f}-r_{2g}\right)\cdot\left(r_{1f}+r_{2g}\right)}{\left|r_{1f}\right|+\left|r_{2g}\right|}\right) \tag{3.6}$$

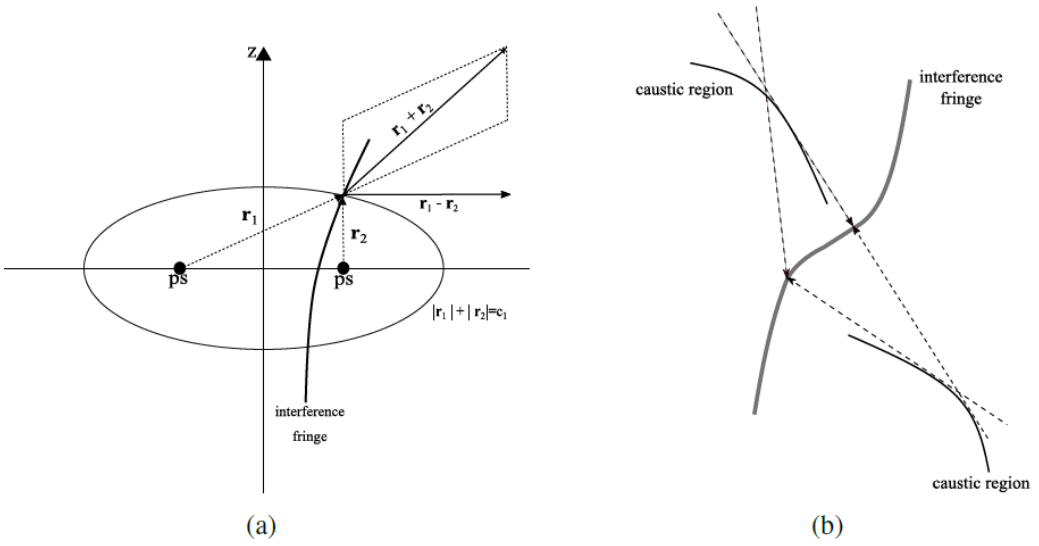

Figure 3.6: Geometric description of interference fringes with the caustic region as a reference.

It is possible to identify two interesting properties:

- A phase jump occurs when the tangent vectors pass through the cusp point.

- In areas where three or more trajectories pass (multivalued regions), the interference structure generates bifurcation effects.

$$k\left(|\mathbf{r_{if}}| - |\mathbf{r_{jg}}|\right) = k\left(\frac{\left(\mathbf{r_{if}} - \mathbf{r_{jg}}\right)\cdot\left(\mathbf{r_{if}} + \mathbf{r_{jg}}\right)}{|\mathbf{r_{if}}| + |\mathbf{r_{jg}}|}\right) \quad 1, j = 1, 2, \ldots n \tag{3.7}$$

The focal region act as source/sink of the optical field

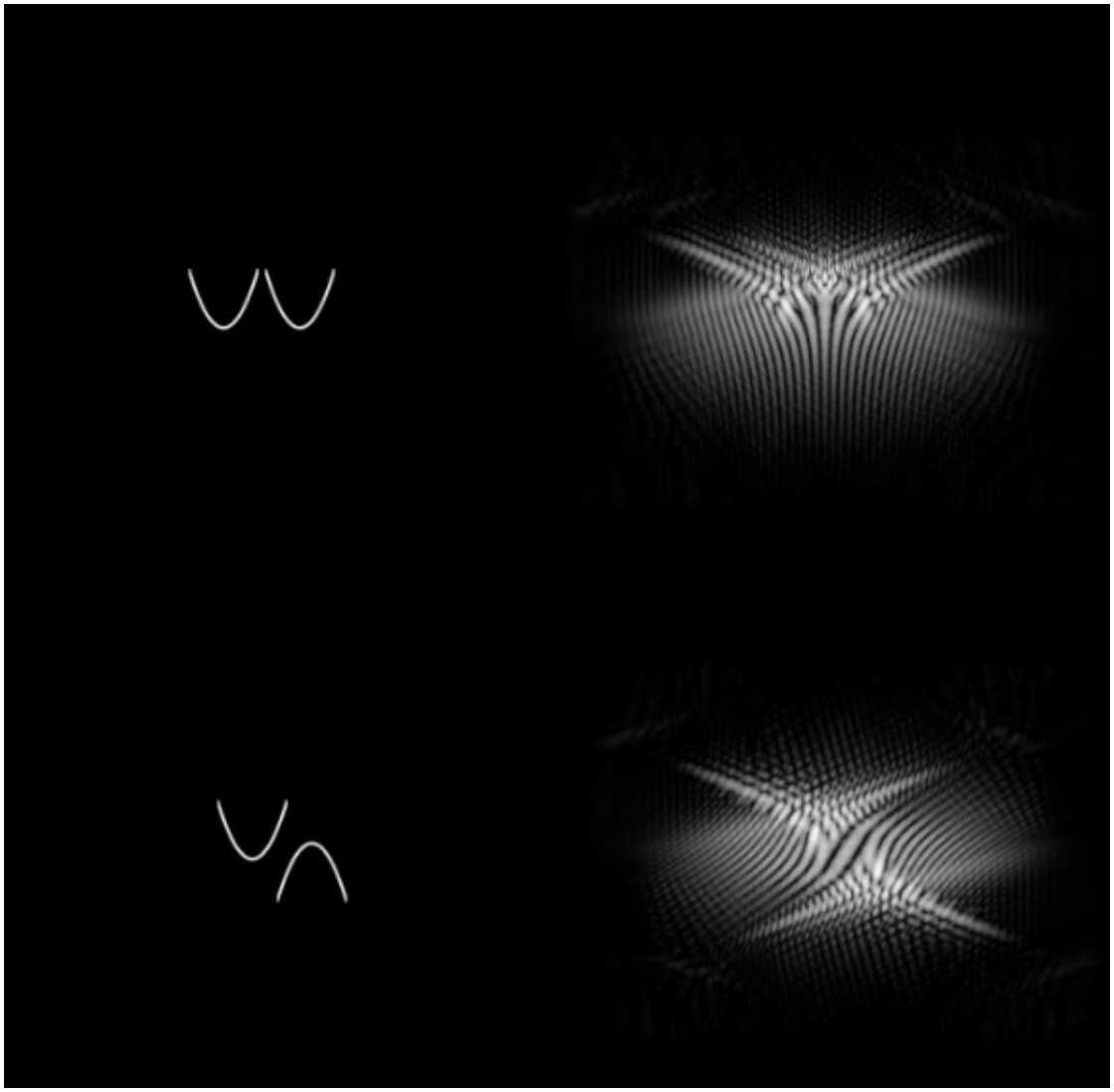

Figure 3.7: Young-Pearcey interferometer in different configurations and its corresponding interference pattern.

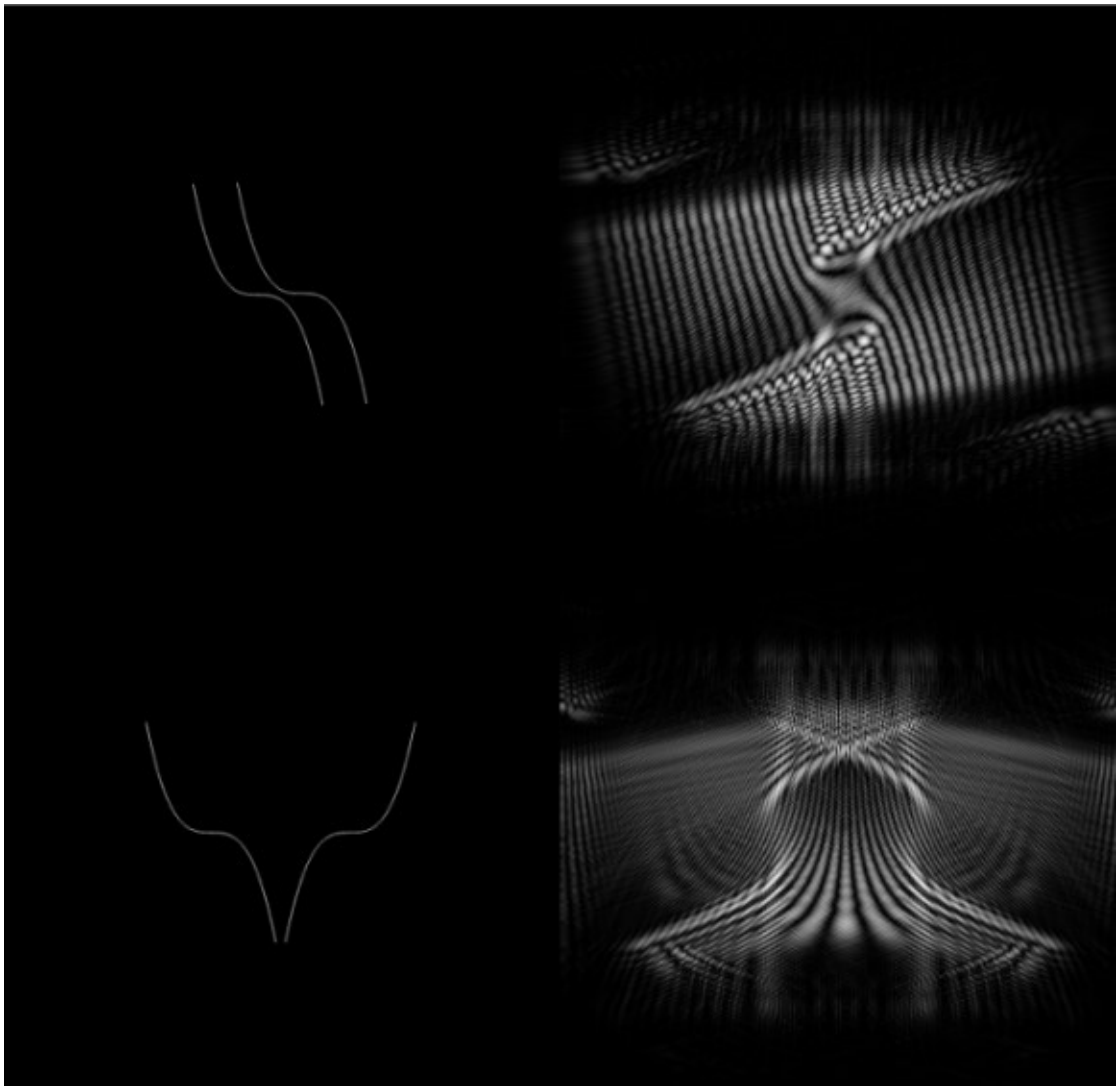

Figure 3.8: Young-Airy interferometer in two possible configurations and its corresponding interference pattern.

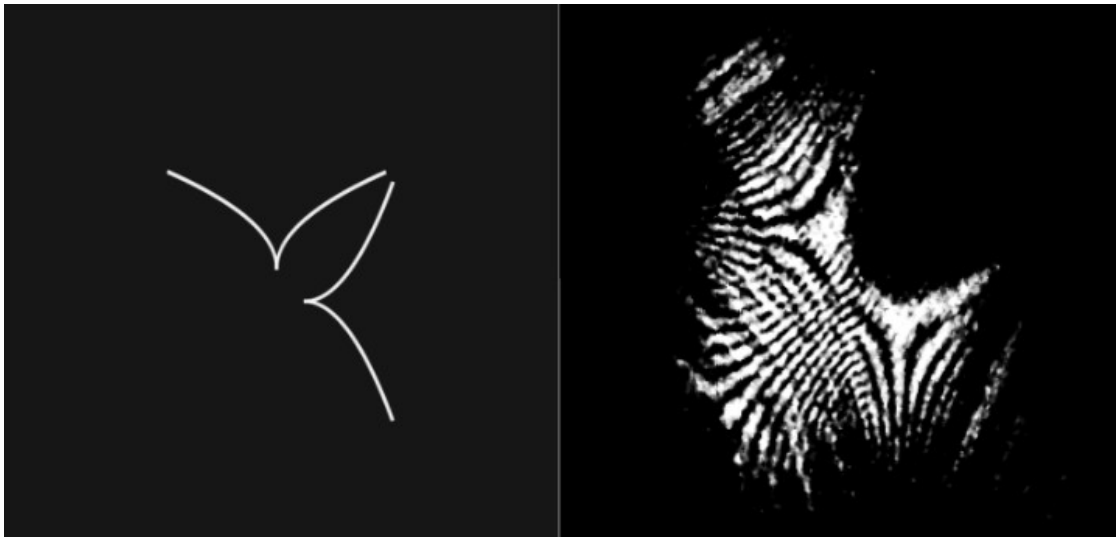

Figure 3.9: Young-cusp interferometer in two possible configurations and its corresponding interference pattern.

The fringe folding process cannot be analyzed from the amplitude function, so an analysis in irradiance is proposed.

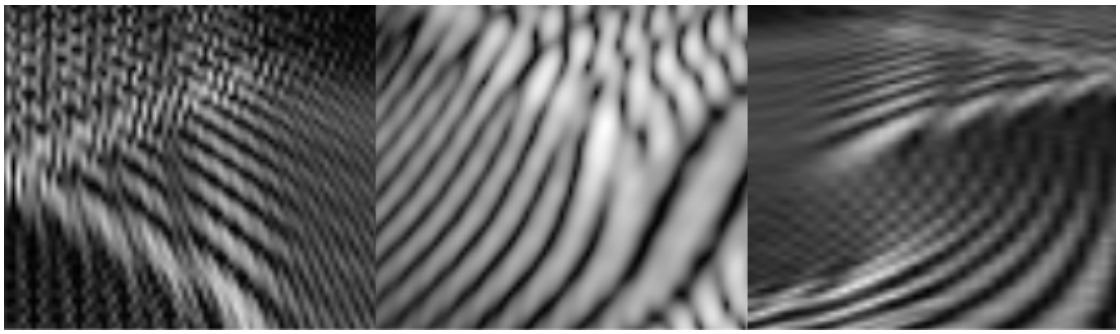

Figure 3.10: Irradiance interaction between the interference fringes and the caustic region. Each lobe of the focal region acts as a sink for the interference fringe.

The irradiance interaction between the focal region and the interference fringe can be modeled using the logistic equation with harvesting

$$\frac{dI_1}{dt} = -aI_2 - bI_1I_2 \tag{3.8}$$

$$\frac{dI_2}{dt} = cI_1 + dI_1I_2 \tag{3.9}$$

Where I_1 is the irradiance of the focal region and I_2 is the irradiance of the interference fringe. The irradiance transfer should depend on the value of the irradiance of the interference fringe (form factor), which can be described by the correlation function between the caustic region and the interference fringe. The minus sign indicates that the irradiance should transfer from the focal region (maximum energy) to the interference fringe.

$$\frac{d\left(I_1 - I_2\right)}{dt} = \left(I_1 - I_2\right)\left(h + e\left(I_1 - I_2\right)\right) + \left(gI_1^2 + mI_2^2\right) + cI_1. \tag{3.10}$$

Chapter 4

Stability of focusing regions and its vortex-solitonic properties

As previously mentioned, focusing regions are the singular solutions to the amplitude function of optical fields and are generated by the envelope curve of a set of critics points, which can be of attractor or repulsor type; its nature depends on the refractive index; a relevant property of these points is that they present charge-like features.

During the time/spatial evolution of the optical field, morphogenesis processes can appear; these processes are associated with effects, such as the Gouy phase, which consists of a shift in the phase function when the optical field is compressed [10, 11]. In our case, maximum compression occurs in the focus regions, and the irradiance function acquires particle-like properties that may generate diffusion features [12, 13].

For a better understanding, it is important to analyze diffusion when it occurs in a random media refraction index. When a focusing region is in a random refractive index medium, current-like effects appear and its evolution acquires diffusive behavior; its morphology may generate vortices or "eternal solutions" of solitonic type in a non-linear medium.

Moreover, the fact that the non-linearities evolve, generating focusing regions, allows us to associate these non-linearities with the boundary condition by changing the curvature function. Through interference effects and the resulting fringes, the behavior of the critical points, which can be of attractor or repulsor type [14], can be revealed and the charge-like properties appear. This last statement is corroborated by the interaction between two types of optical fields Pearcey [15]. Here, the condition under which these effects occur is analyzed and experimentally corroborated.

4.1 PDE and focusing regions

Wave properties are associated with hyperbolic partial differential equations that have two characteristic curves; so, to generate wave diffusion transitions it is necessary to induce bifurcation effects on the characteristic curves [16]. Furthermore, diffusion processes are associated with parabolic partial differential equations that possess only one characteristic curve, which is in keeping with the one-dimensional character of the focusing regions [17].

The refractive index can modify the nature of the critical points and induce bifurcation effects. Hence, attractor points can become repulsor critical points and inversely. The other case is when the attractor points can cancel with repulsor critical points. The proposed physical model on where the phase term disappears implies that the irradiance distribution does not satisfy the wave partial differential equation, but a diffusion equation, commonly proved by using Fick's law, does it. Its known that all physical systems evolve towards an equilibrium configuration. In this context, the critical points must reach a stable configuration.

To reach this configuration, we propose to modify Fick's law by adding some non-linear terms. These terms will be associated with a canonical form of three different kinds [14]: node-point, Pitchfork bifurcations, and transcritical bifurcations. Experimentally, a node-point means that the interaction between the attractor and repulsor points cancels one another. Thus, no singularities exist and the focusing region must be dissipated in the media. Pitchfork bifurcations occur when the stability term is cubic, and the optical fields can be associated with the generation of vortex-like behavior. Lastly, in the transcritical bifurcations, the canonical form is of the logistic type. Thus, the asymptotic behavior generates "eternal solutions" as described in [18, 19, 20], which correspond to soliton-type solutions. Therefore, the stability points reverse their behavior from attractor to repulsor.

The switch in their behavior generates a current of critical points. In a dynamical system, the attractor points move in opposite directions of the repulsor points, corresponding to two characteristic curves, and the optical field presents wave effects. Once the system reaches a stable configuration, the solitonic solution appears. The latter is in agreement with the Gaponov-Grekhov statement: "Caustics are the first cousin of solitons" [21].

We describe this dynamic by performing two types of experiments. The first one analyzes the interaction between two optical fields and shows that focusing regions act as attractors or repulsors for the interference fringes presenting charge-like properties. The second experiment describes the propagation of FR in a random refractive index media; this makes it evident that the three kinds of canonical form can occur. For this study, the optical field is described by a set of trajectories with an associated vector field that satisfies the continuity equation. Each

trajectory must satisfy extremal features, and global properties of the vector field must satisfy the transversal condition [22]. The interference effects, generated in the neighborhood of the focusing region, produced charge-like properties, and the transversal condition cannot be fulfilled, and the diffusion effects acquire one-dimensional behavior. The study analyzes the geometrical evolution of an optical field. The amplitude function is generated using a slit-shaped curve as a boundary condition, and it has associated a vector field $\vec{F}$ given by

$$\vec{F} = \mu \nabla \phi, \tag{4.1}$$

where $\mu(n)$ is function of the refractive index and ϕ is the phase function. Taking the divergence of (4.1) we obtain

$$\nabla \cdot (\mu \nabla \phi) = \frac{\partial \phi}{\partial t} = \mu \nabla^2 \phi + \nabla \mu \cdot \nabla \phi. \tag{4.2}$$

The (4.2) has a simple geometric interpretation as is shown in Fig. 4.1, where two regions are identified. In region I, none of the trajectories intersect each other. Therefore $\nabla \mu \cdot \nabla \phi = 0$, which is the mathematical representation of the transversal condition. Consequently, the phase function satisfies the Laplace equation [23], and (4.2) is rewritten as $\nabla^2 \phi = 0$. In region II, some trajectories intersect each other. The intersection generates interference effects. Thus, the resulting optical field divergence is different from zero and the transversal condition is not fulfilled. This effect can be deduced in a polarized plane wave propagating along z coordinate given by $\vec{E}(z) = (a, b) \exp(ikz)$, where a and b are complex constants. Implementing a rotation along the y axis, it is easy to show that the expression for the sum of two plane waves whose resultant wave vector is placed on the $x - z$ plane is given by:

$$\begin{aligned} \vec{E}(x, z) = (E_x, E_y, E_z) = (a \cos\theta, b, -a \sin\theta) \exp(ik\gamma) \\ + (d \cos\theta, e, d \sin\theta) \exp(ik\beta), \end{aligned} \tag{4.3}$$

where $\gamma = x \sin\theta + z \cos\theta$ and $\beta = -x \sin\theta + z \cos\theta$. The expression for the resulting wave is:

$$\begin{aligned} E_x(x, z) = \cos\theta \sqrt{|a|^2 + |d|^2 + 2|ad| \cos(2kx \sin\theta)} \\ \exp\left[\tan^{-1}\left(\frac{a \sin\gamma + d \sin\beta}{a \cos\gamma + d \cos\beta}\right)\right]. \end{aligned} \tag{4.4}$$

The expressions for the E_y and E_z components are analogous to E_x. We emphasize the fact that the divergence of the resulting interfered field is different from zero, this means that charge-like effects are induced. We can identify the charge features from the periodical distribution of the interference fringes. We will show that by controlling the boundary condition, a charge distribution oc-

curs in focusing regions. The fact that divergence is different from zero results from the complex function not being analytical. Consequently, it does not satisfy the Cauchy-Riemann conditions. This means that the derivative of the amplitude function depends on the trajectory. This can be understood from Fig. 4.1. In region II two or more trajectories are intersected generating interference and the derivative on the intersection point depends on the trajectory chosen. (4.2) can be rewritten as

$$\nabla \cdot \vec{F} = h(x), \tag{4.5}$$

or equivalently

$$\nabla^2 \phi = \frac{1}{\mu}(h(x) + \nabla\mu \cdot \nabla\phi), \tag{4.6}$$

where the phase function for the interfered optical field presents charge-like properties. It must be noted that $\nabla\mu \cdot \nabla\phi \neq 0$. So, the transversal condition for the flow of $\vec{F}$ is not satisfied, because all trajectories of $\vec{F}$ are tangent to the focusing region [24].

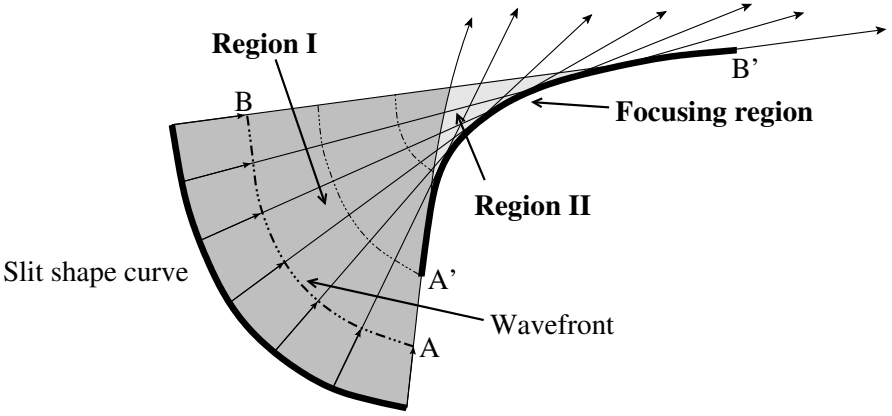

Figure 4.1: The trajectories emerge perpendicular to the slit shape curve. The envelope of the trajectories corresponds to the focusing region. Two regions can be identified: In region I no trajectory intersects. In region II some trajectories are intersected generating interference effects and charge-like features.

A relevant point consists of identifying the charge-like properties by analyzing the interference between two Pearcey-kind optical fields. This type of optical field emerges from a transmittance that consists of a slit-shape parabolic curve [25], whose representation is:

$$\begin{aligned} \vec{E} &= \iint \vec{\xi}(x,y)\delta(y-x^2)\frac{\exp(ikr)}{r}dxdy \\ &= \int \vec{\xi}(x)\exp[c(z)(x^4 + x_0x^2 + y_0x)]dx, \end{aligned} \tag{4.7}$$

where $\vec{\xi}(x) = (a(x), b(x), c(x))$ is an amplitude vector. The interference expressions for the interference between two Pearcey-kind optical fields are obtained when we put two slit shape curves as the transmittance function, given by $t(x, y) = \delta(y - (x^2 - a)) + \delta(y - (x^2 + a))$. The expression for the resulting electric field is:

$$\vec{E} = \int \vec{\eta} \exp\left[\frac{i\pi}{\lambda z}(x^4 + x^2(1 - 2y_0) - 2xx_0 + a^2)\right] \cos\left[\frac{2a\pi}{\lambda z}(x^2 - y_0)\right] dx, \tag{4.8}$$

$\vec{\eta}(x)$ is the resulting amplitude vector. We used a Michelson interferometer, where the incident optical field was a Pearcey-kind beam generated by illuminating a transmittance containing a parabolic slit with a He-Ne laser. The experimental results are shown in Fig. 4.2 for different mirror tilts. It is evident that the focusing region acts as a source or a sink for the interference fringes, corroborating the charge-like properties. The next point consists in analyzing the stability properties of focusing regions in a media with a time-dependent refractive index, (4.1) can be related to irradiance properties, noting that

$$\mu \nabla \phi \cdot \Delta l_{AB} \hat{N} = I_{A'} - I_{B'} \quad , \tag{4.9}$$

where Δl_{AB} is a length element on the wavefront and $\hat{N}$ is a unitary vector normal to Δl_{AB}. Dividing by a differential arc length Δs of the focusing region.

$$\frac{\mu \nabla \phi \cdot \hat{N} \Delta l_{AB}}{\Delta s} = a \frac{I_{A'} - I_{B'}}{\Delta s}, \tag{4.10}$$

must be noted that the terms Δl_{AB}, Δs have different metrics, consequently, when the wavefront is mapped on the focusing region, an irradiance distribution is generated. Taking the limit when $\Delta s \to 0$ (4.10) acquires the form

$$\frac{\partial I}{\partial s} = f(I) = aI + bI^2 + cI^3 + \ldots \quad , \tag{4.11}$$

where the linear term of this equation constitutes the optical version of Fick´s law. Satty has proposed a similar description to describe the diffusion effects of the Liouville flow in cryptodeterminism processes [25]. Considering only linear features and supposing that the flow is changing with time, then (4.10) takes the form

$$D \frac{\partial^2 I}{\partial s^2} = \frac{\partial I}{\partial t}, \tag{4.12}$$

which corresponds with the diffusion equation. The Fick´s law can be related with

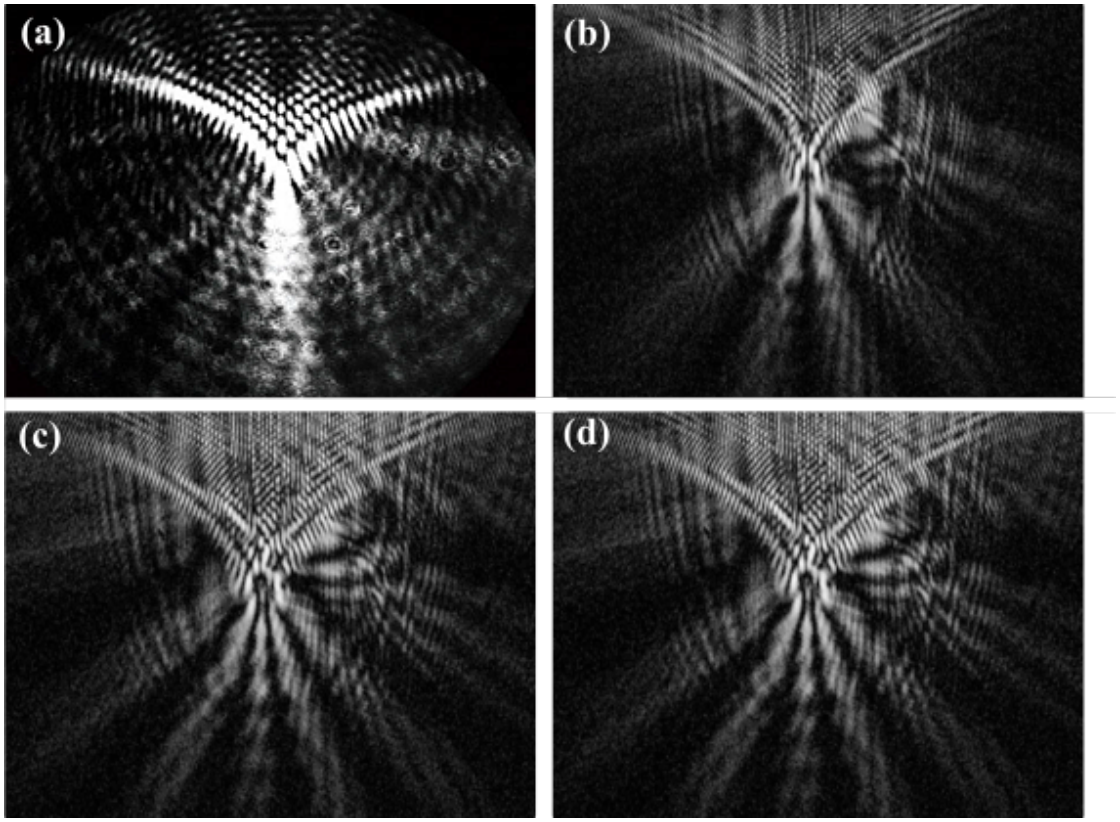

Figure 4.2: (a) Focusing region of a Pearcey- kind optical field emerging from a parabolic slit shape transmittance. (b)-(d) Experimental results of the interference between two focusing regions. The interference fringes are organized around focusing regions which can act as sources or sinks.

temporal changes, noting that

$$\frac{\partial I}{\partial s} = \frac{\partial I}{\partial t}\frac{\partial t}{\partial s} = \frac{1}{v}\frac{\partial I}{\partial t}. \tag{4.13}$$

The relevance of (4.12) is that the irradiance distribution has particle-like properties. This is expected because the irradiance function does not carry information about the phase function. Solving the linear diffusion equation (4.12), the irradiance function takes the form of

$$I(s,t) = m(t)\exp(as). \tag{4.14}$$

When the parameter a is negative, the irradiance is reabsorbed in the media. Interesting features appear when the nonlinear terms are considered: the decreasing exponential behavior can be balanced when the nonlinear terms are considered. This generates an asymptotic behavior for the irradiance function, which is ana-

lyzed from Fick's law with nonlinear terms.

In dynamic systems, different types of singularities can appear of atractor or repulsor kind. To corroborate the behavior of the critical points, we experimentally analyzed the propagation of an incoherent plane wave through a medium with a random refractive index, we make use of this kind of source to avoid interference effects. This is due to the fact that the proposed theoretical model is based on irradiance behavior. The medium with a random refractive index was generated by continuously adding isopropyl alcohol drops to a water container (1 drop per second). The medium was illuminated with an incoherent plane wave, and the irradiance evolution was recorded with a CCD camera Fig.4.3.

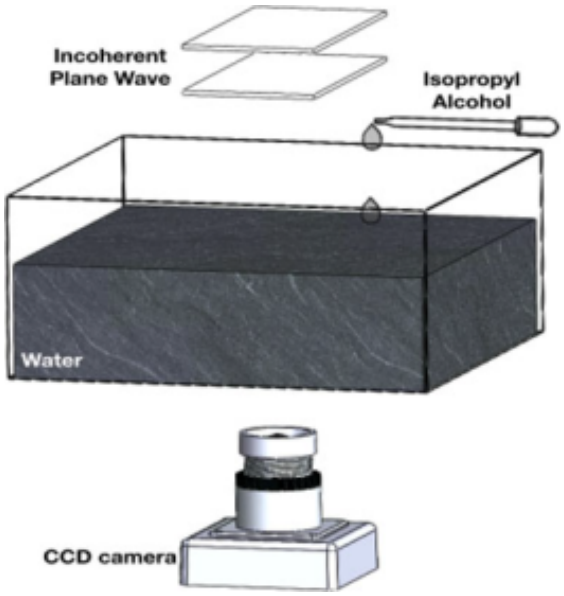

Figure 4.3: Alcohol drops modify the refractive index in a random way; this modifies the curvature function of the wavefront. The wavefront propagation generates focusing regions.

With previous experimental setup was possible to identify three different types of bifurcation: **nodepoint**, **pitchfork bifurcations**, and **transcritical bifurcations**. These appear due to the fluctuations of the refractive index, and the bifurcations will randomly appear at a given moment. Experimental results are shown in Fig.4.4 and Fig.4.5. The canonical forms are as follows [5]:

a) the node-point is the simplest case. The critical points disappear, and the focusing region is reabsorbed. A repulsor point cancels an attractor point. Mathematically, Fick's law takes the form:

$$\frac{\partial I}{\partial t} = a_1 I + b_1 - I^2. \tag{4.15}$$

The critical points are obtained when $a_1 I + b_1 - I^2 = 0$, and the solution to the quadratic equation shows that two real critical points are obtained when $a_1^2 - 4b_1 > 0$ is satisfied, and a bifurcation is generated when $b1 = 0$. Therefore, the critical points collide and cancel each other. For this case, the irradiance is quickly transferred to the media.

b) Pitchfork bifurcation: for this case, Fick's law takes the form

$$\frac{\partial I}{\partial t} = a_1 I + b_1 I^2 + c_1 I^3. \tag{4.16}$$

and therefore, there are three critical points. One of them is an attractor (I=0), and the remaining two are repulsors. In polar coordinates, the focusing regions are exponential trajectories rotating around the attractor point. Thus, the trajectory of the focusing regions acquires a spiral shape, as shown in Fig. 4.4.

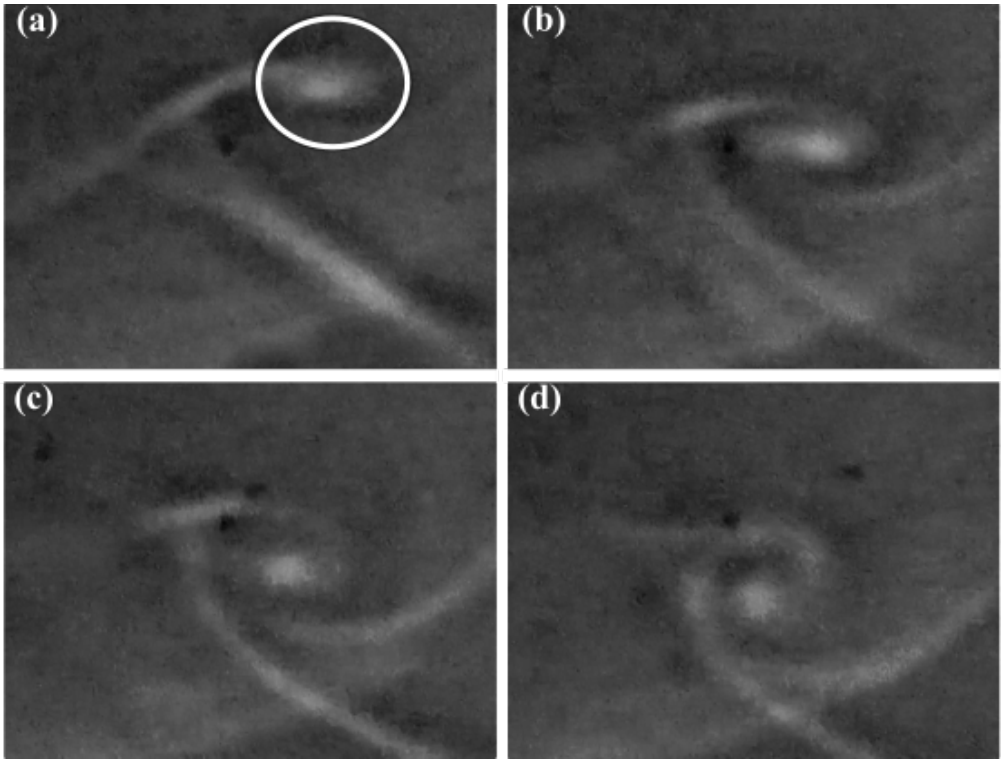

Figure 4.4: Generation of optical vortices for a bifurcation-type pitchfork. (a) Initial focusing region. As time evolves, the highlighted point shows an attractor behavior, and the trajectories of the focusing regions curve towards it, generating a vortex effect. (b)–(d). Geometry of the focusing regions is in very good agreement with the work presented by Strogatz [5] for the pitchfork bifurcation.

Herein, an interesting behavior can be observed in the highlighted bright point. This point has 'zero speed', which corroborates its attractor behavior: all trajec-

tories move towards it following vortex-like geometries.

c) Transcritical points: this case occurs when Fick's law takes the form:

$$\frac{\partial I}{\partial t} = a_1 I + b_1 I + c_1 I^2. \tag{4.17}$$

Here, the critical points do not disappear, but change their behavior from repulsor to attractor and vice versa. In a dynamic system, the transcritical points generate a current-like behavior. The asymptotic behavior generates **"eternal solutions"** of the solitonic kind, as shown in Fig.4.5.

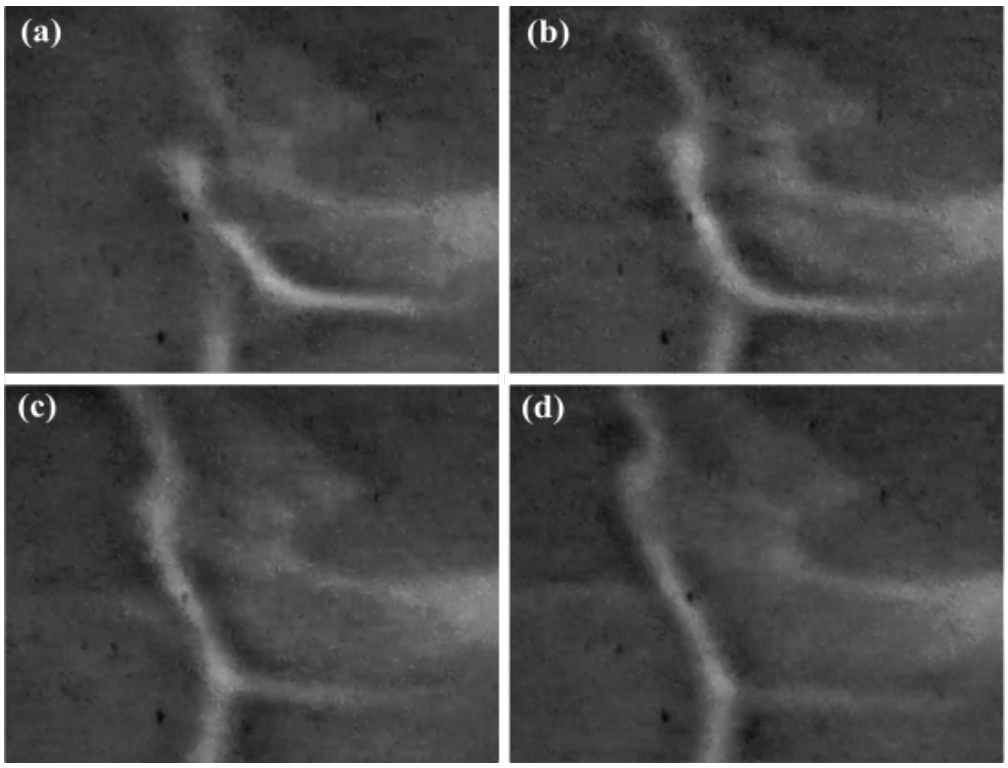

Figure 4.5: Organization of focusing region tending to generate solitonic features. (a) Initial structure of the focusing region. After time progresses, a self-organization appears (b), and the diffusion effects stretch the focusing region. At a longer time period, the focusing region geometry evolves towards a linear shape, which corresponds to solitonic properties (c), (d).

The behavior of these focusing regions is strongly similar to the Ricci solitons [9].

Chapter 5

Conclusions

First, we give a brief context of what a focusing region is, how it is possible to generate it, and what kind of properties it has. Also, we explain two different approaches to explain it, the geometrical optics explanation and the physical optics point of view. In both, the place that plays the curvature function is relevant to the generation of an interesting physical effect that occurs in the neighboring of it, this effect, is that we called wave-diffusion processes.

Also, it was possible to show that the focusing regions act as sources or sinks for the interference fringes. Thus, the focusing regions present charge-like properties. The theoretical model was experimentally proved with an set of interferometrical experiments.

By means of the topological Young interferometer, performed with two quadratic or cubic slits, it was possible to identify how the irradiance flux of an interference finge, and the direction in which the interference finge is formed, both are in perpendicular directions. An interesting fact related to the geometry is that a phase jump occurs when the tangent vectors pass through the cusp point and that in areas where three or more trajectories pass (multivalued regions), the interference structure generates bifurcation effects, i.a. The focal region acts as a source/sink of the optical field. The folding process that the fringe experiment cannot be analyzed by means of the amplitude function, so,in this way, irradiance analysis is necessary.

When the optical field propagates in a medium with a random refractive index, a current-like property is observed that satisfies the diffusion equation. Therefore, the attractor or repulsor nature of the critical points can be controlled with the refractive index. Hence, the geometry of the focusing regions depends on the kind of critical points. In this work, we identify three types of critical point and describe them by stabilizing Fick's law. These critical points were also experimentally detected.

Point-node critical points showed that the focusing regions are reabsorbed by the media. Pitchfork bifurcation critical points generate vortex-type geometries, and transcritical critical points generate 'eternal solutions' that correspond to solitonic-type solutions. The experimental results agree with the non-linear terms added to the Fick law. Future work consists of analyzing the behavior of Fick's law on the focusing regions propagated in nonlinear media and understanding the conditions in which Ricci solitons are generated. Additionally, this work can be implemented for the generation of tunable waveguides. These can be obtained by illuminating the focusing regions with variable wavelengths. Further work needs to be performed to demonstrate the previous statement, also the study of focusing regions on partially coherent fields, and the interaction with stochastic/Markovian beams being on board in future works.

List of Figures

Bibliography

[1] CORNELIUS LANCZOS. *The Variational Principles of Mechanics*. University of Toronto Press, 1962.

[2] M.V. Berry. The adiabatic phase and pancharatnam's phase for polarized light. *Journal of Modern Optics*, 34(11):1401–1407, 1987.

[3] Vasudevan Lakshminarayanan, Ajoy K. Ghatak, and K. Thyagarajan. *The Optical Lagrangian and the Ray Equation*. Springer US, Boston, MA, 2002.

[4] Don S. Lemons. *Perfect Form: Variational Principles, Methods, and Applications in Elementary Physics*. Princeton University Press, 1997.

[5] Alain J Brizard. *INTRODUCTION TO LAGRANGIAN AND HAMILTONIAN MECHANICS*. Department of Chemistry and Physics Saint Michaels College, Colchester, 2004.

[6] D.J. Struik. *Lectures on Classical Differential Geometry*. Addison-Wesley series in mathematics. Addison-Wesley Publishing Company, 1961.

[7] M.V. Berry and C. Upstill. *IV Catastrophe Optics: Morphologies of Caustics and Their Diffraction Patterns*, volume 18 of *Progress in Optics*. Elsevier, 1980.

[8] Andreas Mandelis. *Diffusion-Wave Fields*. Springer, 01 2001.

[9] Gabriel Martinez-Niconoff, Jazmin Carranza, and Alejandro Cornejo-Rodriguez. Caustics of diffraction fields. *Optics Communications*, 114(3):194–198, 1995.

[10] P. Hariharan and P. A. Robinson. The gouy phase shift as a geometrical quantum effect. *Journal of Modern Optics*, 43(2):219–221, 1996.

[11] Jun Yang and Herbert G. Winful. Generalized eikonal treatment of the gouy phase shift. *Opt. Lett.*, 31(1):104–106, Jan 2006.

[12] G. Martinez Niconoff, P. Martinez Vara, S. I. De los Santos Garcia, M. A. Torres-Rodriguez, M. Vargas Morales, and E. Saldivia Gomez. Analysis of wave-diffusion transitions in optical fields. *Journal of Modern Optics*, 65(20):2290–2294, 2018.

[13] Orad Reshef, Philip Camayd-Munoz, Daryl I. Vulis, Yang Li, Marko Loncar, and Eric Mazur. Direct observation of phase-free propagation in a silicon waveguide. *ACS Photonics*, 4(10):2385–2389, 2017.

[14] S.H. Strogatz. *Nonlinear Dynamics and Chaos: With Applications to Physics, Biology, Chemistry and Engineering*. Studies in nonlinearity. Westview, 2000.

[15] James D. Ring, Jari Lindberg, Areti Mourka, Michael Mazilu, Kishan Dholakia, and Mark R. Dennis. Auto-focusing and self-healing of pearcey beams. *Opt. Express*, 20(17):18955–18966, Aug 2012.

[16] E.J. Beltrami. *Mathematics for Dynamic Modeling*. Academic Press, 1987.

[17] P. Garabedian. *Partial Differential Equations*. AMS Chelsea Publishing Series. Chelsea Publishing Company, 1986.

[18] Zhaosheng Feng. Traveling wave behavior for a generalized fisher equation. *Chaos, Solitons and Fractals*, 38(2):481 – 488, 2008.

[19] P.G. Drazin, R.S. Johnson, D.G. Crighton, M.J. Ablowitz, S.H. Davis, E.J. Hinch, A. Iserles, J. Ockendon, and P.J. Olver. *Solitons: An Introduction*. Cambridge Texts in Applied Mathematics. Cambridge University Press, 1989.

[20] Richard S. Hamilton. Eternal solutions to the ricci flow. *J. Differential Geom.*, 38(1):1–11, 1993.

[21] A.V. Gaponov-Grekhov and M.I. Rabinovich. *Nonlinearities in action: oscillations, chaos, order, fractals*. Springer-Verlag, 1992.

[22] L. Elsgoltz. *Differential equations and the calculus of variations*. MIR Publishers, 1977.

[23] T.L. Saaty. *Modern Nonlinear Equations*. Dover Books on Mathematics Series. Dover Publications, 1981.

[24] Gabriel Martinez-Niconoff, Jazmin Carranza-Gallardo, A. Cornejo-Rodriguez, and E. Ley-Koo. Design of projective zone plates and their focusing properties. *Opt. Lett.*, 22(9):594–596, May 1997.

[25] P. Martinez-Vara, J. Silva Barranco, S. I. De Los Santos G., J. Munoz-Lopez, M. A. Torres-Rodriguez, R. Suarez Xique, and G. Martinez-Niconoff. Diffraction by three-dimensional slit-shape curves: decomposition in terms of airy and pearcey functions. *Opt. Lett.*, 40(15):3496–3499, Aug 2015.